Chapter 4
Pharmaco-Imaging in Translational Science and Research

Immanuel Freedman

Abstract Examples of pharmaco-imaging in translational science and research include whole body infrared imaging of normal healthy mouse, magnetic resonance imaging of normal healthy mouse calf muscle, and magnetic resonance imaging of relapsing-remitting multiple sclerosis patient brain. Rationales, experimental design, study outcomes, and conclusions are presented.

4.1 Introduction

Within GSK Biopharm & Immuno-inflammation Pharmacoology, studies are performed on biopharmaceutical compounds in preclinical models such as mice, rats, and monkeys, as well as humans from First Time in Human to Post-Marketing (phases I–IV).

Aligned with the vision of GlaxoSmithKline Clinical Pharmacology, Modeling, and Simulation to establish model-based technology as a core element of the drug development process, the Biopharm & Immuno-inflammation Pharmacology group integrates pharmacokinetics, pharmacodynamics, modeling, simulation, and biometrics into the selection, global development, and registration of drugs for the betterment of patients.

Mechanistic pharmacometric models, typically based on nonlinear mixed modeling methods, may enable translation between compounds, species, phases, therapeutic areas, and indications, considering their similarities and clinically significant differences, and translation of terms in mathematical models.

I. Freedman (✉)
GlaxoSmithKline, King of Prussia, PA, USA
e-mail: immanuel.q.freedman@gsk.com

B.R. Moyer et al. (eds.), *Pharmaco-Imaging in Drug and Biologics Development*,
AAPS Advances in the Pharmaceutical Sciences Series 8, DOI 10.1007/978-1-4614-8247-5_4,

Noninvasive methods such as imaging may increase the number of observations that can be made without significantly perturbing the biological system by invasive blood draws or stressful biopsies. This chapter discusses specific examples of pharmaco-imaging methods with demonstrated value in internal and regulatory decision-making.

4.2 Specific Examples: Example 1: Whole Body Infrared Imaging of Normal Healthy Mouse

4.2.1 Rationale

Osteoarthritis (OA) is a widely prevalent joint disease with a high unmet medical need that represents a substantial economic burden. In OA, cartilage metabolism outpaces anabolic regeneration with consequent destruction of cartilage. Aggrecan is a key structural component of cartilage, responsible for elasticity, water content, and structural integrity. ADAM TS 5 is an enzyme expressed by chondrocytes that degrades aggrecan, and ADAM TS 5 activity is linked to the development and progression of OA in both mouse models and human OA.

This section discusses pharmaco-imaging methods that demonstrate preclinical target engagement and pharmacokinetics and provide translational guidance for an unspecified monoclonal antibody (mAb) directed against ADAM TS 5.

4.2.2 Materials and Methods

4.2.2.1 Animal Model: Normal Healthy Hairless (SHK1) Mouse

Mouse IgG1 isotype control (MOPC21) or unspecified anti-ADAM TS 5 monoclonal antibody (mAb) was labeled with IR800 green fluorescent dye in phosphate-buffered saline (PBS) solution. They were administered to normal healthy hairless (SHK1) mice via the intraperitoneal (IP) or intra-articular (IA) route ($n = 6$/group) as follows:

• Mouse IgG1 isotope control	225 μg in 200 μL	PBS IP
• Anti-ADAM TS 5 mAb	225 μg in 200 μL	PBS IP
• Mouse IgG1 isotype control	50 μg in 15 μL	PBS IA
• Anti-ADAM TS 5 mAb	50 μg in 15 μL	PBS IA

The mice were serially imaged at 800nm wavelength, bled following administration, and $n = 3$ mice/group were sacrificed at 8 days and 60 days after dose. The in vivo time course of whole body mAb biodistribution and total and ADAM TS 5-specific pharmacokinetics in serum was determined by near-infrared imaging on the LI-COR Odyssey scanner (LI-COR Biosciences:NE).

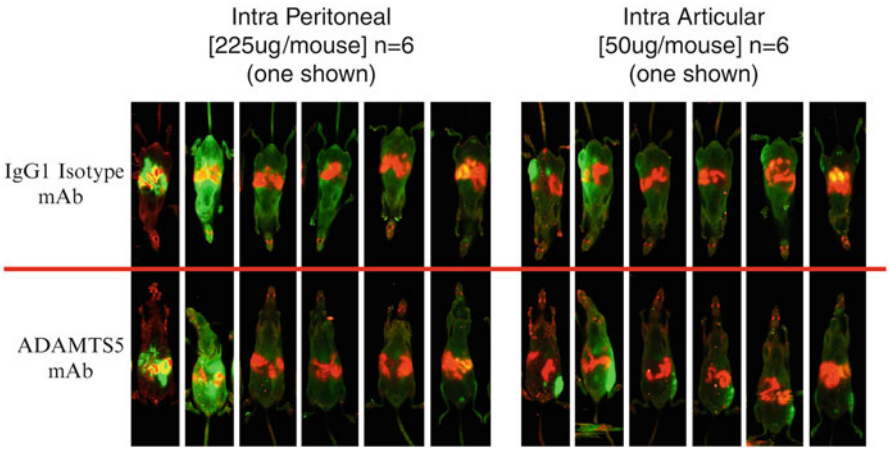

Fig. 4.1 Image sequence showing time course of single-dose IgG1 isotype mAb and anti-ADAM TS 5 mAb biodistribution in SHK1 mouse at 0.5, 24, 72, 168, 672, and 1,344 h after dose

4.2.2.2 Standard Curves

Qualitative standard curves for IR800-labeled IgG1 isotope control (MOPC21) and anti-ADAM TS 5 mAb were imaged according to the following protocol at serial dilutions from 1:1 to 1:32 for initial concentrations of 299 and 319 μg/mL, respectively.

- Co-incubate 10 μL of labeled mAb in PBS with 10 μL protein A/G beads (Thermo Scientific:IL) for 30 min at 25 °C in a 96-well v-bottom microtiter plate.
- Add 100 μL PBS.
- Centrifuge plate and aspirate liquid.
- Wash beads 3× with 100 μL PBS and aspirate liquid.
- Read plate on LI-COR Odyssey imaging system.

4.2.3 Results and Discussion

4.2.3.1 Whole Body Biodistribution

Figure 4.1 shows the time course of whole body biodistribution for one of $n=6$ mice, suggesting a longer half-life for the anti-ADAM TS 5 mAb dosed at 50 μg IA than 225 μg IP.

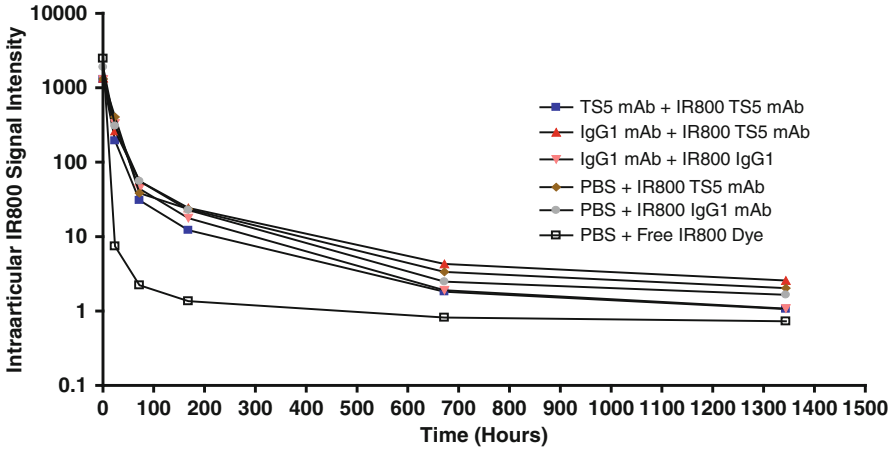

Fig. 4.2 Labeled mAb pharmacokinetics after unlabeled mAb administration

Table 4.1 Labeled mAb pharmacokinetics after unlabeled mAb administration

Compound	$t_{½,\alpha}$ (h)	$t_{½,\beta}$ (h)
TS5 mAb + IR800 TS5 mAb	12.7	511
IgG1 mAb + IR800 TS5 mAb	9.13	221
IgG1 mAb + IR800 IgG1	39.6	NC
PBS + IR800 TS5 mAb	13.1	483
PBS + IR800 IgG1 mAb	8.1	89.2
PBS + IR800 PBS	2.87	101

NC not calculated

4.2.3.2 Labeled mAb Challenge After Unlabeled mAb Administration

Figure 4.2 shows the time course of anti-ADAM TS 5 mAb pharmacokinetics following 0.2 mg unlabeled mAb on day 1 and 0.1 mg labeled mAb on day 1 administered via the IA route. Compartmental pharmacokinetic analysis with WinNonlin 5.2 software (Pharsight:NC) yields a two-compartment linear model with nominal distributional half-life $t_{½,}\alpha$ and terminal half-life $t_{½,}\beta$ according to Table 4.1.

4.2.3.3 Translation to Human

Table 4.1 and Fig. 4.2 suggest target engagement since the anti-ADAM TS 5 mAb has longer half-life than the IgG1 isotype control at the same dose. By allometric scaling of passive processes (Savage et al. 2004; West et al. 1997), a nominal 483 h terminal half-life for the fluorescent signal from 0.1 mg *total* anti-ADAM TS 5 mAb

dosed via the IA route to 25 mg mouse scales to 60 kg human according to $(60{,}000/25)^{1/4} \times 483$ h = 3,380 h (140 days), while a nominal 89.2 h terminal half-life for the 0.1 mg IgG1 isotype control scales to 624 h (26.0 days), in reasonable agreement with a typical 21-day serum terminal half-life for non-binding mAb in human.

4.2.3.4 Limitations

Limitations of this method include (a) the animal size is limited to the physical size of the Odyssey scanner, (b) continuous observations in vivo require gas anesthesia, and (c) the fluorescent signal strength standard curve is qualitative.

4.3 Example 2: Magnetic Resonance Imaging of Normal Healthy Mouse Calf Muscle

4.3.1 Rationale

Myostatin is a secreted protein that inhibits muscle differentiation and growth. Encoded by the myostatin gene (MSTN), myostatin is produced in skeletal muscle cells and circulates in blood as free mature myostatin and as an inactive latent complex of the myostatin C-terminal dimer and other proteins including its propeptide. Mature myostatin acts on muscle tissue by binding a cell-bound activin R2 receptor. Humans lacking a functional MSTN gene, MSTN knockout, and conditional knockout mice gain muscle mass, while transgenic mice that overexpress MSTN selectively in skeletal muscle lose muscle mass.

Overexpression of myostatin may be implicated in human muscle-wasting diseases including hip fracture and cancer cachexia. A therapeutic humanized mAb that binds mature myostatin may increase human muscle mass by competitive antagonism of the muscle growth inhibition that occurs when mature myostatin binds the activin R2 receptor.

This section discusses pharmaco-imaging methods that demonstrate preclinical target engagement and pharmacokinetics and provide translational guidance for an unspecified monoclonal antibody (mAb) directed against mature myostatin.

4.3.2 Materials and Methods

4.3.2.1 Animal Model: Normal Healthy ♂ C57BL/6 Mouse

Mouse IgG2a isotype control or an unspecified murine mAb (10B3) directed against mature myostatin was administered to normal healthy ♂ C57BL/6 mice 8 weeks

old, via the intraperitoneal (IP) route on days 0, 4, 7, 14, and 21 at 10 mL/kg concentration for day 0 to reduce dose volume and 5 mL/kg for the remaining doses, $n = 6$/group, as follows:

• Mouse IgG2a isotope control	30 mg/kg IP (Group 1)
• Anti-myostatin mAb (10B3)	3 mg/kg IP (Group 2)
• Anti-myostatin mAb (10B3)	30 mg/kg IP (Group 3)

The mice were serially imaged by magnetic resonance image (MRI) on a weekly basis for 12 weeks following initial dosing. Contours were manually drawn around muscle, excluding bone and subcutaneous fat. Calf muscle volumes were recorded weekly, and cardiac septum and left ventricular wall thickness were recorded based on an average of three measurements at the day 0 and weeks 2, 4, and 12 time points. Serum pharmacokinetic samples and animal body weights were collected weekly from day 0 to week 12. Tissue samples including leg and heart muscles were collected for analysis at week 4.

4.3.2.2 MRI Instrumentation and Method

A Bruker BioSpec 4.7T 40 cm MRI Scanner (Bruker: MA) scanned the mice. The scans were enhanced with T2 contrast enhancement, using a multi-echo spin-echo sequence based on Rapid Acquisition with Refocused Echoes (RARE) factor of 4. Four averages were obtained, with repetition time 1,500 ms and echo time 8 ms. Motion suppression was enabled. The matrix size was 256×192 with field of view 4×4 cm. The slice thickness was 0.75 mm and total acquisition time 4′48″ for each calf muscle observation.

4.3.3 Results and Discussion

Figure 4.3 shows the percent change from baseline for calf muscle volume from day 0 to week 12 with treatment period from day 0 to week 4 and washout period from weeks 4 to 12.

4.3.3.1 Pharmacometric Model Development

Serum pharmacokinetics of the10B3 mAb obtained from a satellite study of male C57BL/6 dosed with 0.1, 1, or 10 mg/kg single dose IP ($n = 4$/time point) were well described by a mamillary model with (1) depot, (2) serum, and (3) peripheral compartments. In Fig. 4.4, the PK model is described by absorption rate constant (Ka), central volume of distribution (V1), linear clearance (K), Michaelis-Menten maximal velocity (Vm) and serum concentration at half-maximal velocity (Km)

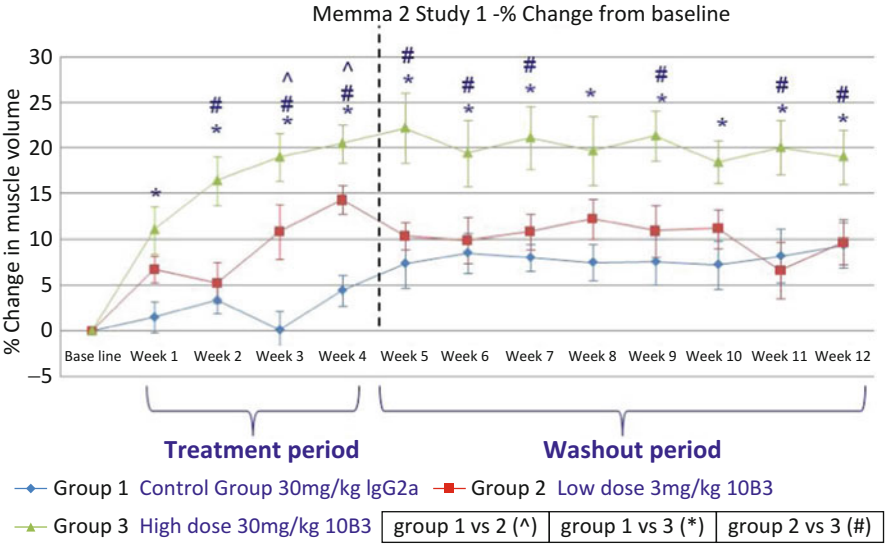

Fig. 4.3 Calf muscle volume percent change from baseline from day 0 to week 12 with treatment period from day 0 to week 4 and washout period from weeks 4 to 12 for C57BL/6 male mice dosed with 3 or 30 mg/kg 10B3 or IgG2a control IP on days 0, 4, 7, 14, and 21

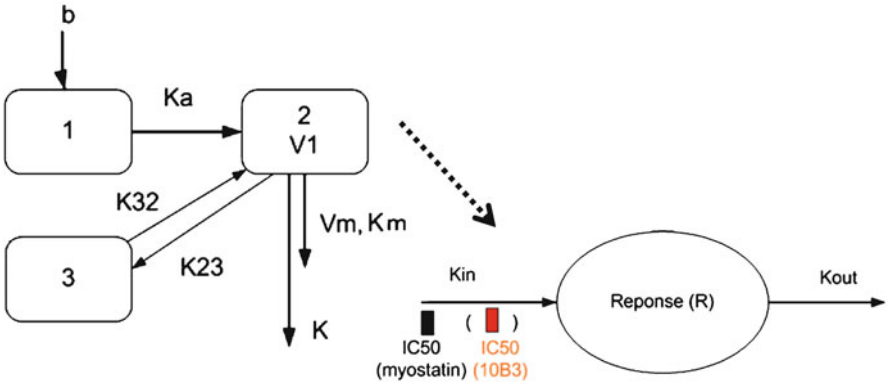

Fig. 4.4 Sequential indirect response pharmacometric model with competitive antagonism

(Gibiansky et al. 2008), central-to-peripheral rate constant (K23), and peripheral-to-central rate constant (K32).

Since the mAb (10B3) is a competitive antagonist of a negative regulator of muscle growth (myostatin), the time course of calf muscle growth in male C57BL/6 mice was well described by a sequential indirect response pharmacometric model (Sharma and Jusko 1998) developed in NONMEM VI software (ICON: NJ). The model structure is depicted in Fig. 4.4, where 10B3 antagonizes the negative muscle growth regulation of myostatin in terms of Loewe additive response.

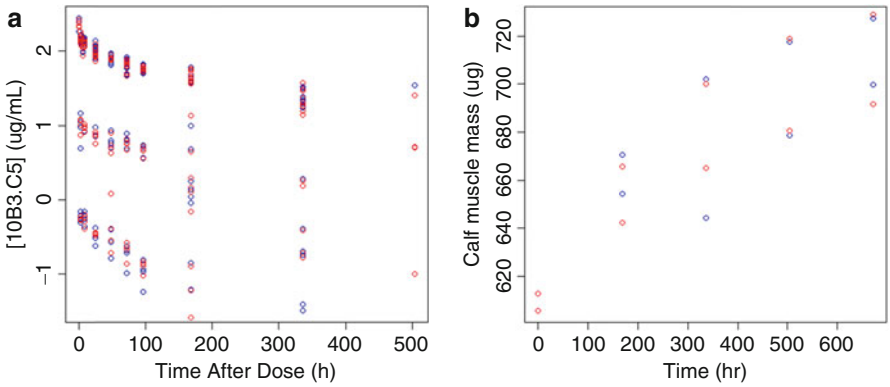

Fig. 4.5 Observed and predicted mean (**a**) PK in male C57BL/6 mice dosed with 0.1, 1, or 10 mg/kg IP single dose ($n=4$/time point) and (**b**) calf muscle volume PD profile in male C57BL/6 mice dosed with 3 or 30 mg/kg on days 0, 4, 7, 14, and 21 ($n=6$/group) (*blue* observed, *red* predicted)

The natural muscle growth response is produced at an input rate constant (Kin) and turns over at output rate constant (Kout). Myostatin inhibits muscle growth with serum concentration at half-maximal inhibition (IC50,myostatin) while 10B3 antagonizes myostatin at half-maximal concentration (IC50, 10B3); PD model parameters include the maximal inhibition of muscle growth (Imax) and maximal muscle growth (Emax). Since the mice are growing, the PD model may not be in initial homeostasis.

Figure 4.5 shows good agreement between the observed and predicted mean PK profile in male C57BL/6 mice dosed with 10B3 0.1, 1, or 10 mg/kg IP single dose ($n=4$/time point) and observed and predicted calf muscle volume PD profiles in male C57BL/6 mice dosed with 10B3 3 or 30 mg/kg IP on days 0, 4, 7, 14, and 21.

The maximal lean muscle mass decrease versus increase of soleus, gastrocnemius, quadriceps, and tibialis anterior muscle for sedentary myostatin transgenic and conditional knockout mice relative to wild-type mice at necropsy was well described by a straight line of slope 0.706 ± 0.198, with adjusted $R^2 = 0.79$. The muscle mass increase is in qualitative agreement with the mean cross-sectional area of Type 2 muscle fiber in C57BL/6J mouse soleus, gastrocnemius, and tibialis anterior muscles (Fig. 4.6) (Augusto et al. 2004).

4.3.3.2 Translation to Human

The target therapeutic profile requires that efficacious treatment of patients with 25 % muscle loss should reverse the muscle loss within 24 weeks of treatment with onset of clinical benefits within 5 weeks after first dose.

Each parameter in the PK/PD model was translated from 25 g mouse to 70 kg human according to allometric scaling of passive processes (Mager et al. 2009) to

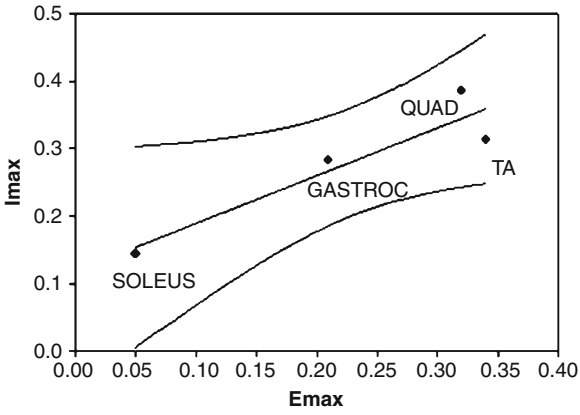

Fig. 4.6 Maximal muscle mass decrease (Imax) versus increase (Emax) for sedentary myostatin transgenic and conditional knockout mice. The *curved lines* represent a 90 % prediction interval

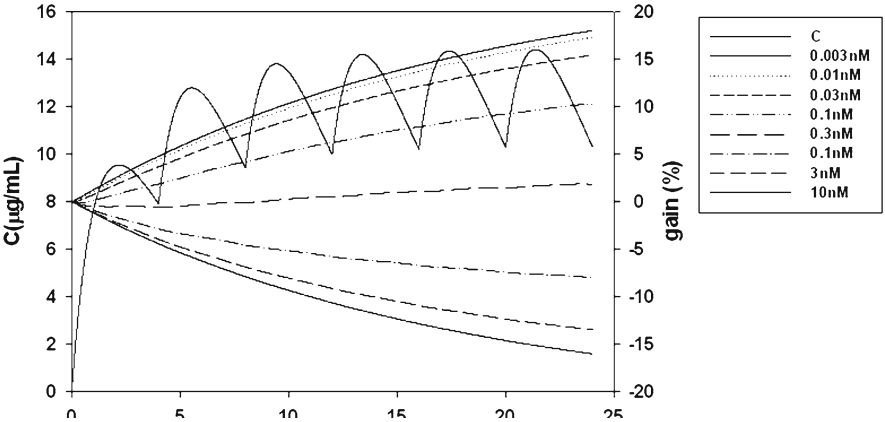

Fig. 4.7 Predicted gain in gastrocnemius muscle mass by design IC_{50} for 70 kg human disease model dosed with 5 mg/kg every 4 weeks for 24 weeks

provide a predictive PK/PD model using Berkeley Madonna software (University of California, Berkeley, CA).

Figure 4.7 shows the PK and predicted gain in gastrocnemius muscle mass for a 70 kg diseased human with initial myostatin levels sufficient for almost maximal muscle wasting (25 %), dosed with 5 mg/kg every 4 weeks for 24 weeks of a prospective humanized mAb directed against myostatin, where the linear regression shown in Fig. 4.6 translated the predicted gain in tibialis anterior (calf) muscle mass to gastrocnemius muscle mass.

According to the target therapeutic profile, efficacious treatment with therapeutic mAb directed against myostatin may require the development of a humanized mAb with 0.03–0.1 nM affinity.

4.3.3.3 Limitations

Limitations of this method include (a) the MRI instrumentation may limit the size of animal that may be imaged, (b) the development of a pharmacometric model requires mechanistic understanding of the biological effect and drug metabolism, and (c) translation of the pharmacometric model to human requires assumptions about scaling and careful consideration of interspecies similarities and differences.

4.4 Example 3: Magnetic Resonance Imaging of Relapsing-Remitting Multiple Sclerosis Patient Brain

4.4.1 Rationale

Multiple sclerosis (MS) is a multifocal, heterogeneous, progressive neurological disease characterized by inflammation, demyelination, and gliosis of the central nervous system (CNS). Although the etiology of MS remains unknown, convergent lines of genetic, immunological, and epidemiological evidence suggest that tissue injury results from a misdirected immune response triggered by "nonself" antigens that mimic constitutive peptides of myelin. Relapsing-remitting multiple sclerosis (RRMS) is specifically characterized by unpredictable exacerbation of symptoms (relapse), followed by periods of remission, during which any deficits from the relapse may recover with or without sequelae.

Ofatumumab is a novel IgG1κ lytic monoclonal antibody (mAb) that specifically binds to the human CD20 antigen of which expression is restricted to B lymphocytes from the pre-B-cell stage to the plasmacytoid immunoblast stage only. A recent trial with an anti-CD20 mAb (rituximab) demonstrated that targeting B cells reduces the number of gadolinium-enhancing (GdE) T1 lesions and the relapse rate in relapsing-remitting multiple sclerosis (RRMS). Ofatumumab has been shown to be both well tolerated and efficacious in several diseases, including a small, placebo-controlled trial in RRMS known as OMS11502 (also known as GEN414) (Sorensen et al. 2010).

This section discusses pharmaco-imaging methods that demonstrate clinical target engagement and pharmacokinetics and provide guidance for the design of clinical trial OMS112831 in relapsing-remitting multiple sclerosis patients by translation of ofatumumab from rheumatoid arthritis to relapsing-remitting multiple sclerosis.

4.4.2 Materials and Methods

1. Human model: patient with relapsing-remitting multiple sclerosis.
2. Imaging method and materials.

Subjects received monthly MRI brain scans from screening to 48 weeks after first dose, followed by an individualized follow-up period. Imaging analysts counted the number of new T1 Gd-enhancing lesions and new or enlarging T2 lesions at each scan relative to the previous scan.

4.4.3 Results and Discussion

Study OMS112831 is a double-blind, placebo-controlled, parallel-group study that will investigate the safety and efficacy of a subcutaneous formulation of ofatumumab in the treatment of subjects with RRMS. The primary objective of the study is to investigate efficacy as assessed by magnetic resonance imaging. Other objectives will include evaluation of tolerability/safety, dose-response relationship, pharmacokinetics, pharmacodynamics, exposure-response, as well as other clinical endpoints.

Figure 4.8 shows raw summary statistics for ofatumumab study OMS115102 (GEN 414) that highlight the minimal amount of observed new MRI lesion activity following administration of IV ofatumumab in both the week 0–24 and week 24–48 treatment periods. Although driven largely by one subject with 88 lesions, the mean number of new T1-weighted GdE lesions for the overall placebo group was 9.69 lesions. The effect of ofatumumab on total T1-enhancing lesions, new and/or enlarging T2 lesions, and new T1 hypointense lesions with very low MRI activity in treated subjects was similar to that seen on new T1 GdE lesions.

The only available data on subcutaneous ofatumumab administered to human is from the study OFA110867 in rheumatoid arthritis (RA) patients. The majority of adverse events (AEs) in OFA110867 were mild or moderate in intensity. Post-injection systemic reactions (PISRs) were more frequent for the combined active (13/27; 48 %) than placebo (2/8; 25 %) group. Overall, safety data indicate that doses up to 60 mg SC single dose were well tolerated with acetaminophen and antihistamine pre-treatment.

At the relatively low doses projected in study OMS112831, no lesion count dose-response information is available for ofatumumab in any clinical or preclinical model. We designed the trial by clinical trial simulation by translating a pharmacometric disease model for subcutaneously administered ofatumumab from RA to RRMS.

4.4.3.1 Pharmacometric Model Development in Patients with Rheumatoid Arthritis

Data from a rheumatoid arthritis (RA) single SQ dose study (study OFA110867) and a pharmacometric model derived from models submitted to BLA 125,326 form the basis of dose predictions for this protocol. The RA study is the starting point for modeling for four reasons:

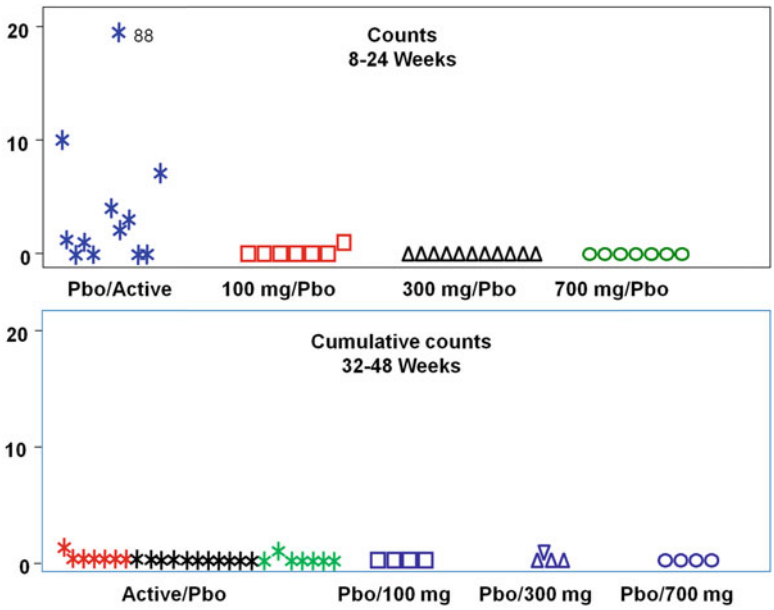

Fig. 4.8 Raw summary statistics for OMS115102 cumulative new T1 Gd-enhancing lesions

- OFA110867 is the only subcutaneously administered ofatumumab study available.
- A unified PK/PD model has been developed from an IV model reported to the FDA for RA, CLL, and FL indications, and this model well describes the relationships between dose, instantaneous concentration, and peripheral CD19+ B-cell count for the RA population.
- The OMS115102 concentration and CD19+ B-cell data do not permit detailed modeling of this PK/PD relationship from OMS115102 data alone.
- The relationship between bioavailability and dose may be complicated by the likelihood that ofatumumab substantially depletes lymphatic B cells before entering systemic circulation.

The choice of the study OFA110867 as basis for modeling likely reflects a conservative viewpoint relative to RRMS. First, the placebo cohort of the OFA110867 study shows peripheral CD19+ B-cell counts that increase with time and may not be in homeostasis because of systemic inflammation related to aggressive lymphoproliferation. Therefore, the same dose to MS patients may result in somewhat higher systemic concentration of ofatumumab and more depletion of peripheral B cells because the peripheral B cells may not proliferate so rapidly in MS as in RA.

4.4.3.2 Translation to Patients with Relapsing-Remitting Multiple Sclerosis

Depleting the $CD20^+$ B-cell subset reduces the supply of mature B cells (including pathogenic B cells) for migration across the blood-brain barrier, clonal expansion, and differentiation into plasma or memory cells.

Kuenz et al. reported that cerebrospinal fluid (CSF) B cells correlated with early brain inflammation in multiple sclerosis including number of GdE lesions, while Petereit et al. observed that reduction in lesion number correlated with reduction in CSF B-cell count (Kuenz et al. 2008; Petereit and Rubbert-Roth 2009).

Kuenz et al. further reported that "new focal white-matter lesions appear to develop following new waves of inflammation, involving immune cells which enter the brain from the peripheral blood and cause major blood-brain barrier leakage mediated by matrix metalloproteinases (MMP)." Sormani et al. reported that the statistical distribution of new GdE lesions observed during a 24-week period was well described by a negative binomial distribution with expected value $\mu = 13.0$ and over-dispersion parameter $\Theta = 0.52$ in RRMS patients not required to have enhancing brain lesions at baseline with monthly MRI scanning over 24 weeks (Sormani et al. 2001).

These observations support the notion that selective recruitment of immune cells across the blood-brain barrier occurs in almost discrete events with an average inter-event interval of about 22 weeks, according to a Gamma-Poisson mixture model. The Sormani et al. model provides a statistical link for the mean rate of incidence of new GdE lesions and pharmacometric model predictions of the reduction in count of peripherally activated pathogenic B or T cells that have migrated into the CSF.

Petereit and Rubbert-Roth showed that the observed rituximab plasma to CSF concentration ratio for subjects with a normal blood-brain barrier is about 0.1 %; the expectation for ofatumumab is similar (Petereit and Rubbert-Roth 2009). Normal healthy serum to CSF ratios are about 230:1 for albumin and 369:1 for IgG in the absence of intrathecal IgG synthesis (Tourtellotte 1975). Hence, for subjects with moderate to severe impairment of the blood-brain barrier corresponding to an albumin index of 14–30 (Cook 2006), the ofatumumab plasma to CSF concentration ratio is predicted to be in the range of about 0.87 % to about 1.87 %, based on the *assumption* that plasma to CSF ratios are reasonably close to serum to CSF ratios.

The pharmacometric model therefore postulates a mechanism of lesion formation based on selective recruitment of a very small fraction of pathogenic immune cells across the blood-brain barrier. A key assumption of the kinetics argument is that, if peripheral B cells are implicated in production of the pathogenic immune cells, the production rate of pathogenic immune cells may reasonably be proportional to the instantaneous peripheral B-cell count. If the pathogenic immune cells that have migrated across the blood-brain barrier are implicated in the development of lesions, it is a reasonable kinetic assumption that the production rate of inflammatory (GdE) lesions be proportional to their count, so the cumulative number of inflammatory lesions may be proportional to the exposure to these pathogenic immune cells in CSF.

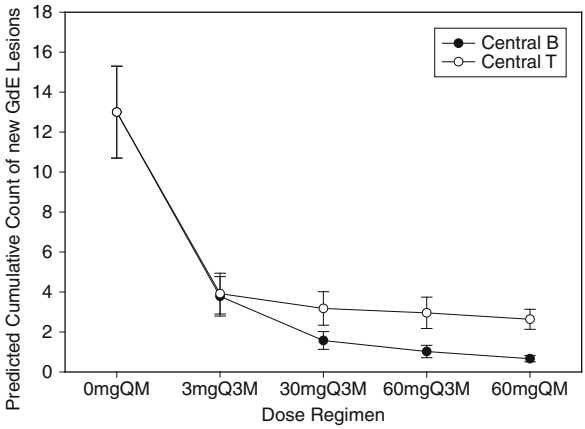

Fig. 4.9 Predicted geometric mean and standard error of estimate of cumulative new Gd-enhancing lesion count over 24 weeks, based on predicted count of peripherally activated pathogenic B or T cells that have migrated into CSF

The model assumes that the T cells are antigen-primed CD4+ cells of CD45RO CCR7^{+} phenotype with mean proliferation and disappearance rates according to Table 2 of Macallan et al. (2004). The uptake rate constants for pathogenic T- or B-cell migration across the blood-brain barrier were based on the respective in vitro migration rates in the presence of both TNF-α and IFN-γ cytokines reported by Alter et al. (2003).

The pathogenic memory B cells are considered to turnover in CSF at the rate estimated for peripheral CD19^{+} B cells in study OFA110867 and to be cleared by ofatumumab by the antibody-dependent cell-mediated cytotoxicity (ADCC) pathway at a rate corresponding to in vitro studies.

The model assumes that pathogenic memory B cells will not proliferate unless they encounter a specific antigen or nonspecific infection that triggers proliferation via antigen binding or toll-like receptor 9 (TLR9) pathways. The model further assumes that the instantaneous mean incidence rate of GdE lesions is proportional to the count of peripherally activated pathogenic T or B cells present in CSF.

The initial distribution of peripheral CD19+ B cells is drawn from a lognormal distribution with expected value $\mu = 198$ GI/L and standard deviation 0.403 on the logarithmic scale obtained by a maximum likelihood fit to the baseline peripheral CD19+ counts observed for the 100 mg cohort of study OMS115102 in RRMS subjects.

Figure 4.9 shows the predicted geometric mean and standard error of new GdE lesions based on the reduction of pathogenic T and B cells present in CSF that have been selectively recruited across the blood-brain barrier via adhesion and the negative binomial distribution for RRMS patients not required to have enhancing brain lesions at baseline, as reported by Sormani et al. (2001).

The pharmacometric model may explain delayed relapse in terms of CSF pathogenic B or T cell proliferation triggered by specific antigen exposure or external event such as infection. In principle, repopulation of peripheral immune cells is necessary but not sufficient for relapse to occur. An external stimulus may be required to trigger rapid proliferation and relapse even after repopulation of CSF B or T cells.

A low uptake rate constant may explain delayed repopulation of pathogenic immune cells in CSF including B cells and T cells. The natural rate of central memory immune cell turnover may explain delayed eradication of pathogenic immune cells from CSF.

4.4.3.3 Dose Rationale

While the 3, 30, and 60 mg single SQ doses were all well tolerated in study OFA110867, the 3 mg single dose was the most tolerable. The OMS112831 study investigates the use of a single 3 mg dose ("conditioning dose") prior to a 30 mg or 60 mg dose in half of the subjects receiving those doses. The intent of the single SQ 3 mg conditioning dose is to reduce cytokine-release reaction to subsequent larger doses by depleting peripheral $CD20^+$ B cells by about 50 % over about 6–9 days, thereby enhancing tolerability.

The purpose of the 3 mg SQ arm is to explore the efficacy of sub-depleting doses (<95 % depletion of peripheral B cells) and to provide information helpful to dose-response and exposure-response modeling. According to the predictive pharmacometric model, the expected reduction of new enhancing T1 lesion burden at week 24 for subjects dosed with placebo at week 0 and 3 mg SQ at week 12 is 55.2 % with 90 % confidence interval 44.7–67.4 %, a response that was observed with currently available first-line MS disease-modifying therapies in their phase II studies. Rituximab data suggest that efficacy in suppressing lesions was maintained through repletion to peripheral B-cell levels ~30 % of LLN (Hauser et al. 2008).

The choice of 30 mg dosed quarterly was because it is the lowest quarterly dose which is likely to continuously maintain at least 95 % peripheral $CD20^+$ B-cell depletion in at least 90 % of the subjects. The choice of 60 mg as the upper dosing cohorts was based on findings that this dose displayed similar peripheral B-cell depletion to 100 mg (the highest dose tested in OFA110867) while appearing to have better tolerability. For the 60 mg monthly cohort, the expected rate of peripherally activated T- and B-cell migration across the blood-brain barrier is very small based on the predicted extensive peripheral B-cell depletion. Although moderate B-cell depletion in the CSF (and perhaps CNS) is possible via ADCC in accordance with the sigmoid Emax model of Bleeker et al., the expectation is that it will not be robust or complete (Bleeker et al. 2007). The 60 and 30 mg arms are expected to deplete peripheral B cells to reduce activation of pathogenic T and B cells (via reduced antigen presentation or regulatory T-cell augmentation) to levels similar to those expected for the efficacious dose in OMS115102 100 mg Q2Wx1. Although the present study duration is only 24 weeks, Fig. 4.10 shows the predicted survival curve for the time to replete peripheral blood CD19+ B cells to LLN (110 cells/μL) after dosing RRMS subjects with SQ ofatumumab in a clinically realistic scenario of treatment discontinuation after one full year of real-world treatment, when steady state has been reached. Note that for doses greater than 3 mg SQ, the predicted time to repletion of peripheral $CD19^+$ B cells to lower limit of normal (LLN: 110 cells/μL) after the last dose exceeds (approximately) 20 weeks. In study OFA110867,

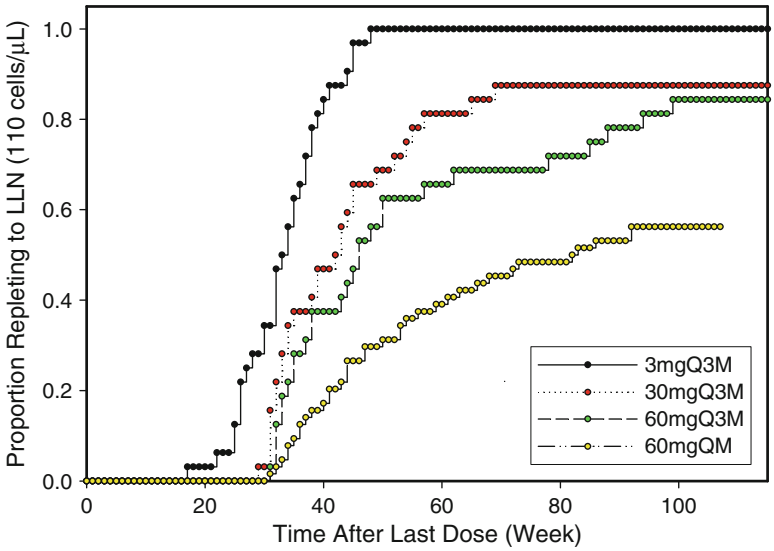

Fig. 4.10 Predicted survival curve for the time to replete peripheral blood CD19+ B cells to LLN (110 cells/μL) in a clinically realistic scenario of treatment discontinuation after 1 full year of real-world treatment

the shortest time to the start of repletion was about 43 days for the 3 mg and 30 mg doses and 57 days for the 60 mg dose, comparable with typical life span of a mature circulating B cell. The OMS112831 doses support dose selection for phase III studies. The predictive pharmacometric model supports a monotonic relation between mean reduction in new enhancing T1 lesion burden and cumulative dose, with 90 % prediction interval including ofatumumab dosed at 10 mg Q3M SQ to 40 mg Q3M SQ for the dose that results in >90 % reduction in new enhancing T1 lesion burden. Repetition of these doses at 3-month intervals, or the lesser of time to repletion of B cells to peripheral LLN, allows partial repletion of peripheral B cells and may provide some level of adaptive immunity against infections (including JC virus variants) that may trigger relapse by opening the blood-brain barrier or by activating pathogenic immune cells expressing TLR9.

4.4.3.4 Limitations

Limitations of this method include (a) the development of a pharmacometric model requires mechanistic understanding of the biological effect and drug metabolism and (b) translation of the pharmacometric model to human requires assumptions about scaling and careful consideration of interspecies similarities and differences.

4.5 Conclusions and Future Directions

Each example highlights the role of pharmaco-imaging to provide noninvasive pharmacodynamic or pharmacokinetic:parmacodynamic (PK/PD is a standard nomenclature) assessments in clinical and preclinical drug development. The detailed relation between short-term assessments and long-term disability measured by clinical score remains to be firmly established in longer-term studies, for translation of muscle hypertrophy in young, growing mice to clinical scores of disability in the sarcopenic hip-fracture patient population and for the relation between lesion counts and clinical scores of long-term disability status such as the Expanded Disability Status Scale (EDSS) in the relapsing-remitting multiple sclerosis patient population.

Acknowledgments The ADAM TS 5 PK study was designed by a GlaxoSmithKline(GSK) team including Elefante, L.; Freedman, I.; Larkin, J.; Liu, F.; Lohr, T.; Matheny, C.; and White, J.

The anti-myostatin PK/PD study "memma2" was designed by a GSK team including Ashman, S.; Chagani, K.; Freedman, I.; and Reid, J.

The OMS112831 study was designed by a GSK team including Bhangu, S.; Carranza, J.; Derosier, F.; Depew, C.; Edwards, T.; Freedman, I.; Grove, R.; Hall, A.; Herrera, P.; Hill-Zabala, C.; Lopez, M.; Nichols, L.; Rogers, R.; Schifano, L.; Schindielorz, A.; Sue-Ling, K.; Tolson, J.; and Watson, D.

References

Alter A, Duddy M, Hebert S et al (2003) Determinants of human B cell migration across brain endothelial cells. J Immunol 170(9):4497–4505

Augusto V, Padovani CR, Campos GER (2004) Skeletal muscle types in C57BL/J mice. Braz J Morphol Sci 21(2):89–94

Bleeker WK, Munk ME, Mackus WJM et al (2007) Estimation of dose requirements for sustained in vivo activity of a therapeutic human anti-CD20 antibody. Br J Haematol 140:303–312

Cook SD (2006) Evidence for an infectious etiology of multiple sclerosis. In: Cook SD (ed) Handbook of multiple sclerosis, 4th edn. Taylor & Francis, New York

Gibiansky L et al (2008) Approximations of the target-mediated drug disposition and identifiability of model parameters. J Pharmacokinet Pharmacodyn 35(5):573–591

Hauser SL, Waubant E, Arnold DL et al (2008) B-cell depletion with rituximab in relapsing-remitting multiple sclerosis. N Engl J Med 358:676–688

Kuenz B, Lutterotti A, Ehling R et al (2008) Cerebrospinal fluid B cells correlate with early brain inflammation in multiple sclerosis. PLoS One 3(7):e2559

Macallan DC, Wallace D, Zhang Y et al (2004) Rapid turnover of effector memory CD4+ T cells in healthy humans. J Exp Med 200(2):255–260

Mager DE, Woo S, Jusko WJ (2009) Scaling pharmacodynamics from in vitro and preclinical animal studies in humans. Drug Met Pharmacokinet 24(1):16–24

Petereit HF, Rubbert-Roth A (2009) Rituximab levels in cerebrospinal fluid of patients with neurological autoimmune disorders. Mult Scler 15(2):189–192

Savage VM et al (2004) The predominance of quarter-power allometric scaling in biology. Funct Ecolo 18(2):257–282

Sharma A, Jusko W (1998) Characteristics of indirect pharmacodynamics models and applications to clinical drug responses. Br J Clin Pharmacol 45(3):229–239

Sorensen PS, Drulovic J, Havrdova E (2010) Magnetic resonance imaging (MRI) efficacy of ofatumumab in relapsing-remitting multiple sclerosis (RRMS)—24-week results of a phase II study. In 26th Congress of the European Committee for Treatment and Research in Multiple Sclerosis (ECTRIMS), Oct 13–16, 2010 , Gothenburg: SE

Sormani MP, Bruzzi P, Rovaris M et al (2001) Modelling new enhancing MRI lesion counts in multiple sclerosis. Mult Scler 7:298–304

Tourtellotte WW (1975) What is multiple sclerosis? Laboratory criteria for diagnosis. In: Davison AN, Humphrey JH, Liversedge AL et al (eds) Multiple sclerosis research, HMSO, London, p 9

West GB, Brown JH, Enquist BJ (1997) A general model for the origin of allometric scaling laws in biology. Science 276(5309):122–126